

AN OPTIMAL POWER MANAGEMENT POLICY FOR HYDROGEN-BASED HYBRID AERO ENGINES

Faezeh Pak[1], Uto Perra[1], Frank Willems[1], Theo Hofman[1] & Mauro Salazar[1]

[1]Eindhoven University of Technology, Eindhoven, The Netherlands. {f.pak, u.perra, F.P.T.Willems, T.Hofman, m.r.u.salazar}@tue.nl

Abstract

In this study we develop an analytical power management policy for a hydrogen hybrid aero engine combining a gas turbine and a solid oxide fuel cell. We use steady-state thermodynamic data to identify convex and concave surrogate models of key subsystem variables through curvature constrained quadratic programming. These models enable the formulation of a partially convex fuel minimization problem, which is later solved analytically using Karush-Kuhn-Tucker conditions and partial convexity and monotonicity model properties. The resulting closed-form policy allows real time optimal power management for each of the flight phases, take off, top of climb and cruise, while respecting operational and thermal constraints. Validation against a high fidelity nonlinear model shows an agreement across take off, climb, and cruise with less than 1.5% normalized root mean square error, demonstrating that the simplified models retain sufficient accuracy for supervisory power management policy. [1]

Keywords: Power management, Optimal control, Solid oxide fuel cell, Gas turbine

1. Introduction

The aviation industry has committed to become climate neutral by 2050, partly by adopting aerospace propulsion concepts. To contribute to the transition toward clean aviation, this study investigates a power management policy for a hybrid electric propulsion system as illustrated in Fig. 1, consisting of a hydrogen gas turbine (GT) and a solid oxide fuel cell (SOFC) that are thermodynamically coupled, to power a propeller via a gas turbine and an electric motor, respectively. This complex aero engine requires a high-level power management policy to coordinate the components' operation and minimize hydrogen consumption while realizing the requested output power. Although the analysis of such a system can be structured either in a steady-state operation or a transient operation, the current work focuses exclusively on the steady-state behavior of the propulsion system during take off, top of climb, and cruise, laying the foundation for future investigations into transient dynamics.

Related Literature: Research in this area spans three streams: (i) control systems for hybrid and conventional aircraft engines, (ii) coordinated control of SOFC/GT integrated systems, and (iii) minimum-fuel strategies in automotive propulsion. In conventional aero-engines, optimization methods such as the maximum principle for the Mayer optimal control problem [3], dynamic programming for power tracking [4], and iterative Hamilton-Jacobi-Bellman reformulations of minimum fuel optimal power tracking during transient operation [5] have been used to improve engine performance. For hybrid SOFC/GT propulsion, PID-based turbine speed control [6] and neural-network multi-loop controllers with optimal tracking [7] have been developed for power tracking rather than fuel-optimal control.

[1]Research funded by the European Union (ID 101138488) and by the UK Research and Innovation (ID 10106893) as a part of the FlyECO project. Views expressed are those of the author(s) only and do not necessarily reflect those of the funding entities. Neither the European Union nor the granting authority can be held responsible for them. [1]

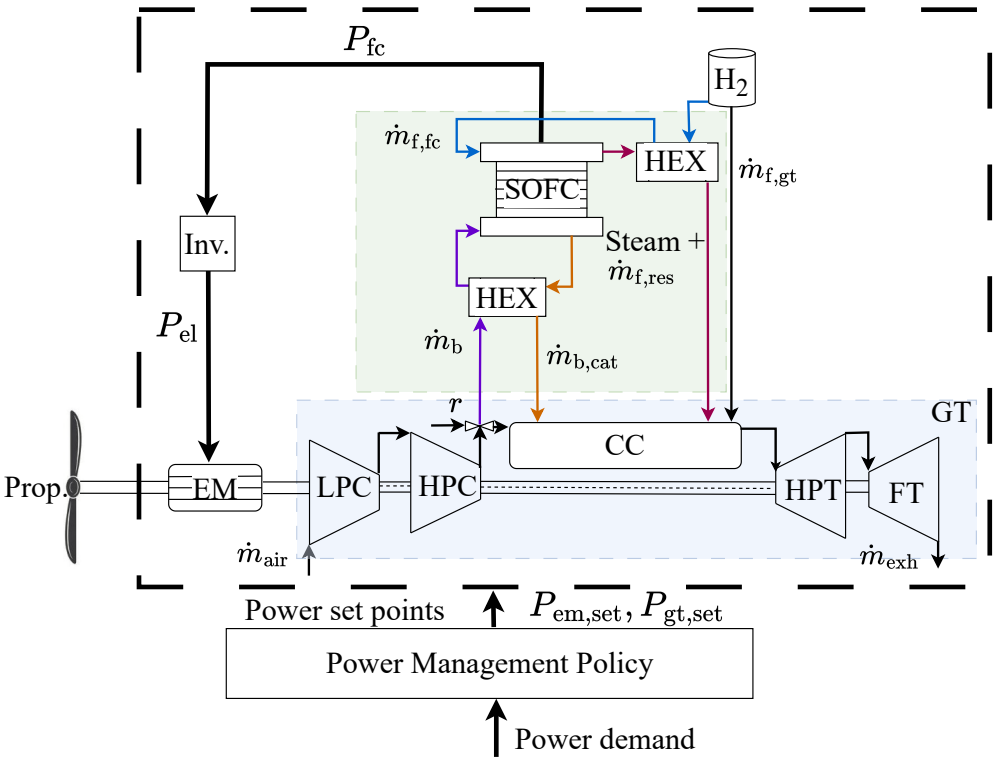


Figure 1 – Simplified schematic view of the aero engine, including a GT, the SOFC, and an electrical motor (EM) [2]. In this figure, $\dot{m}_{f,gt}$ and $\dot{m}_{f,fc}$ are the fuel flow directed to the GT and SOFC, respectively. $\dot{m}_b$ is the bleed air flow, which is guided from the compressor to the SOFC system after warm-up, and $\dot{m}_{f,res}$ is the SOFC off-gas hydrogen. P_{gt}, P_{fc}, and P_{em} are GT output power, SOFC electrical power, and EM power, respectively.

The studies on SOFC/GT configuration in different applications, including in power plants [8], in the marine industry [9], vehicles [10], and in aviation [11], mainly rely on multi-loop coordinated control architectures in which inner-loop controllers regulate the local subsystem dynamics, while an outer-loop controller tracks the required power. In these approaches, power allocation is typically generated by PID controller [12], while the delay in SOFC temperature is not considered, or by optimal approaches using dynamic programming and NLP frameworks for power tracking and maximizing the efficiency [8] or via equilibrium-optimizer algorithms embedded in neural-network-based coordination scheme [9] to avoid local minima in naval warship by fixing the fuel utilization of the SOFC and manipulating the current through changing the fuel flow rate. These controllers focus on meeting power demand rather than computing fuel-optimal supervisory policies for aviation propulsion.

Automotive research offers numerically solved optimal control [13], or analytical optimal control such as ECMS [14], which utilizes Pontryagin's minimum principle (PMP), delivers fast real-time solutions and provides global guarantees under convex formulations [15], and rule-based methods [16] offer robust sub-optimal performance. However, despite their relevance, such optimal supervisory strategies have not been transferred to aerospace hybrid systems, which involve fundamentally different constraints and mission profiles.

Although extensive work exists on power-tracking control, degradation mitigation, and multi-loop coordination for SOFC/GT systems, to the best of the authors' knowledge no prior studies have addressed optimal supervisory power management aimed specifically at minimizing fuel consumption in SOFC/GT hybrid propulsion for aerospace applications. Existing optimal control methods either target efficiency or power tracking rather than fuel minimization, neglect critical SOFC thermal constraints, or have only been applied in automotive or stationary contexts.

Statement of Contribution: In this study we formulate an optimal static feedforward control problem designed to determine such a policy, which is subsequently solved using the KKT conditions. This research makes three main contributions: (i) We identify computationally tractable affine and quadratic

surrogate models of the propulsion system in algebraic formulation by performing a parametric sweep of a high-fidelity simulation of the system in steady state operation. The constraints for the regression curvature ensures that these models maintain the convexity properties for the analytical optimization. (ii) By using the resulted surrogate models with quasi-static approach, we formulate the static fuel minimization problem that incorporates the system's thermal and operational constraints. Notably, by using the monotonicity and curvature behavior of the lifting variables, the problem can be expressed in a convex, one dimensional form. (iii) We eventually derive the optimal power management policy analytically by using the Karush-Kuhn-Tucker conditions, resulting in a closed form supervisory policy that requires no iterative computations. This facilitates the real-time implementation while preserving consistency with physical limits.

Organization: The study is structured as follows: Section 2 outlines the problem and system models. Section 3 describes the optimal control formulation and analytical solution, Section 4 presents the results briefly to validate the methodology, Section 5 suggests future approaches, and Section 6 concludes with key findings and future directions.

2. Problem Statement

This section introduces the propulsion system architecture. Then, we present the system mathematical modeling approach, and then we formulate the objective function and the optimization problem for the optimal control problem.

2.1 System Description

The hybrid propulsion system illustrated in Fig. 1 consists of a GT and an electrical subsystem. The electrical subsystem is composed of an SOFC, an inverter, and an electrical motor. The GT features low- and high-pressure compressor stages (LPC, HPC). A portion of the compressed air is routed to the SOFC cathode after warm-up through a heat exchanger (HEX), while hydrogen is supplied to the anode after a HEX. The electrochemical reactions in the SOFC generate electricity and produce steam. The SOFC off-gases are recirculated to the GT combustion chamber after moving through the HEX, where hydrogen is burned.The recirculation of the air through the propulsion system introduces strong thermodynamic coupling between the GT and the SOFC. The supervisory power management policy determines the power distribution law between the gas turbine and the fuel cell.

2.2 Mathematical Modeling

Based on the steady state dataset, we approximate the key thermodynamic and flow variables, i.e., lifting and input variables, of the hybrid SOFC/GT system using a quasi-static mapping from the gas turbine output power P_{gt} and the SOFC electrical power P_{fc}. For each flight phase, we select the simplest functional form (affine or quadratic) that provides sufficient accuracy while maintaining the convexity and concavity structures of each variable for the subsequent optimization problem. This approach acknowledges that the operating conditions and the dominant system nonlinearities vary substantially between take off, top of climb, and cruise. We interpret each mapping as a reduced-order surrogate of the high-fidelity thermodynamic model, obtained by projecting the steady-state response manifold onto the low dimensional space of $P_{\mathrm{gt}}, P_{\mathrm{fc}}$. Affine coefficients are obtained using

$$\min_{\{\theta_1,\theta_2,\theta_0\}} \sum_{k=1}^{N} \left\| y_k - \left(\begin{bmatrix} \theta_1 & \theta_2 \end{bmatrix} \begin{bmatrix} P_{\mathrm{gt},k} \\ P_{\mathrm{fc},k} \end{bmatrix} + \theta_0 \right) \right\|_2, \tag{1}$$

while quadratic terms subject to curvature constraints are estimated via semidefinite programming of the form shown in Eq. (2)

$$\begin{aligned} \min_{\{Q,\mathbf{q},q_0\}} \sum_{k=1}^{N} & \left\| y_k - \left(\begin{bmatrix} P_{\mathrm{gt},k} & P_{\mathrm{fc},k} \end{bmatrix} Q \begin{bmatrix} P_{\mathrm{gt},k} \\ P_{\mathrm{fc},k} \end{bmatrix} + \mathbf{q}^{\top} \begin{bmatrix} P_{\mathrm{gt},k} \\ P_{\mathrm{fc},k} \end{bmatrix} + q_0 \right) \right\|_2, \\ \text{s.t.} \quad & Q \succeq 0 \text{ or } Q \preceq 0. \end{aligned} \tag{2}$$

The semidefinite constraints on Q enforce convexity or concavity of the quadratic maps, ensuring compatibility with the convex optimal control formulation.

Imposing convex or concave curvature on the surrogate models preserves the structure required for convex optimal control formulations in Section 3., guaranteeing global optimality and efficient solution of the power split optimization problem. The assumptions we consider in the modeling are as follows:

- the inlet temperature for both anode and cathode are identical,
- the outlet temperature for both anode and cathode are identical,
- within each phase, the system performs in steady-state operation. Hence, a quasi-static mapping is appropriate.

The model output vector is

$$\mathbf{x} \coloneqq \begin{bmatrix} \dot{m}_{\mathrm{b}} & \dot{m}_{\mathrm{f,fc}} & \dot{m}_{\mathrm{f,gt}} & T_{\mathrm{in}} & T_{\mathrm{hpc}} & T_{\mathrm{et}} & T_{\mathrm{out}} \end{bmatrix}^{\top}, \tag{3}$$

where T_{in} is the SOFC inlet temperature, T_{hpc} is the HPC temperature, T_{et} is the turbine outlet temperature and T_{out} is the SOFC outlet temperature. Each variable x_j of $\mathbf{x}$ is parameterized either in an affine manner

$$x_j(\mathbf{p}) \;=\; \theta_{j,0} + \boldsymbol{\theta}_j^{\top}\,\mathbf{p}, \tag{4}$$

or in a quadratic form

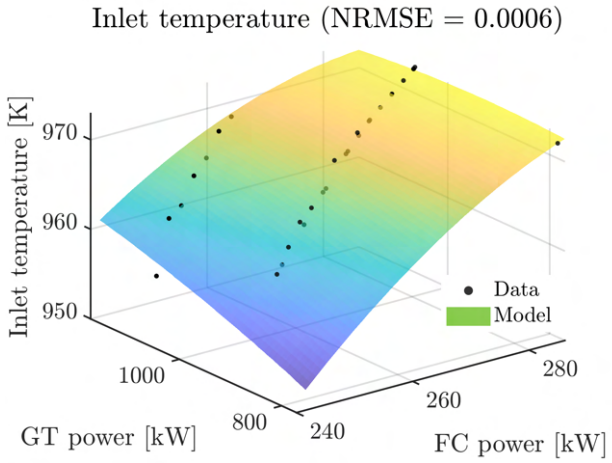
$$x_j(\mathbf{p}) \;=\; \mathbf{p}^{\top} Q_j \mathbf{p} + \mathbf{q}_j^{\top}\mathbf{p} + q_{j,0}, \qquad Q_j \in \mathbb{S}^2, \tag{5}$$

where $\mathbb{S}^2$ denotes the set of 2×2 real symmetric matrices and $\mathbf{p} = \begin{bmatrix} P_{\mathrm{gt}} & P_{\mathrm{fc}} \end{bmatrix}^{\top}$. x_j is convex if $Q_j \succeq 0$ and concave if $Q_j \preceq 0$ and the vector $\mathbf{q}_j = \begin{bmatrix} q_{j,1} & q_{j,2} \end{bmatrix}^{\top}$ and scalar $q_{j,0}$ are fitting parameters. The selection is based on the local nonlinear characteristics of the steady state-data for each flight phase. According to the data distribution for the take off, $\mathbf{x}_{\mathrm{q}} \coloneqq \begin{bmatrix} \dot{m}_{\mathrm{b}} & \dot{m}_{\mathrm{f,gt}} & T_{\mathrm{in}} & T_{\mathrm{hpc}} \end{bmatrix}^{\top}$ have quadratic formulation while $\mathbf{x}_{\mathrm{l}} \coloneqq \begin{bmatrix} \dot{m}_{\mathrm{f,fc}} & T_{\mathrm{out}} & T_{\mathrm{et}} \end{bmatrix}^{\top}$ have linear dependency. For top of climb and cruise quadratic approximation is considered for $\mathbf{x}_{\mathrm{q}} \coloneqq \begin{bmatrix} \dot{m}_{\mathrm{b}} & T_{\mathrm{in}} \end{bmatrix}^{\top}$ and linear approximation for $\mathbf{x}_{\mathrm{l}} \coloneqq \begin{bmatrix} \dot{m}_{\mathrm{f,fc}} & \dot{m}_{\mathrm{f,gt}} & T_{\mathrm{out}} & T_{\mathrm{et}} & T_{\mathrm{hpc}} \end{bmatrix}^{\top}$. The indices q and l indicate quadratic and linear, respectively. We eventually develop piece-wise models with different structure and coefficients during different phases. Model fidelity is assessed using the normalized root-mean-square error (NRMSE) computed over the steady state dataset for each flight phase. Table 1 summarizes the NRMSE values for all lifting variables across take off, top of climb ans cruise. All linear and semi definite programs used for surrogate model identification were solved using MOSEK [17].

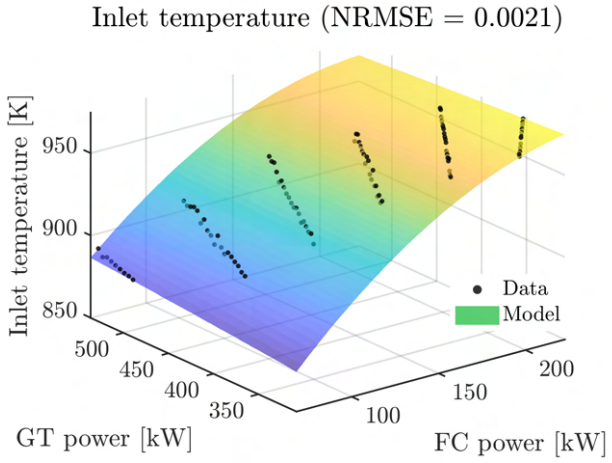
Table 1 – NRMSE for Lifting Variables

Variable	Take off	Top of climb	Cruise
$\dot{m}_{\mathrm{f,gt}}$	0.6%	0.8%	0.9%
$\dot{m}_{\mathrm{f,fc}}$	0.6%	0.2%	0.4%
$\dot{m}_{\mathrm{b}}$	0.6%	1.1%	1.1%
T_{in}	0.06%	0.2%	0.2%
T_{hpc}	0.3%	0.3%	0.2%
T_{et}	0.8%	0.4%	0.3%
T_{out}	0.04%	0.5%	0.4%

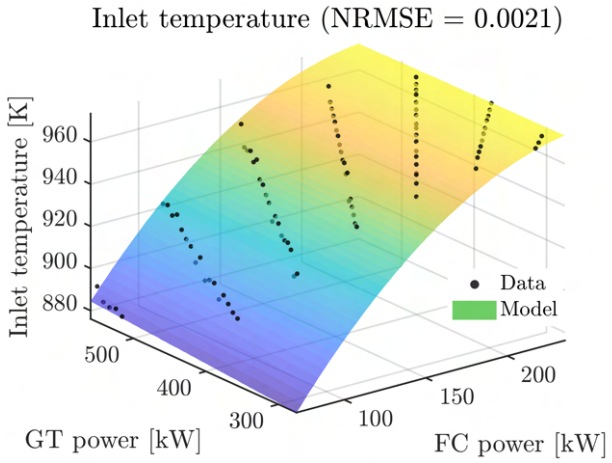
Additionally, Figs. 2, 4 and 6 present three dimensional surface maps illustrating how subsystem power allocation influences key outputs of the propulsion system across different flight phases. The horizontal axes present the values for gas turbine power and fuel cell power, while the vertical axis shows the resulting outputs. These figures exhibit important information about how each variable increases or decreases in response to the change in power distribution between GT and SOFC.



(a) Take off

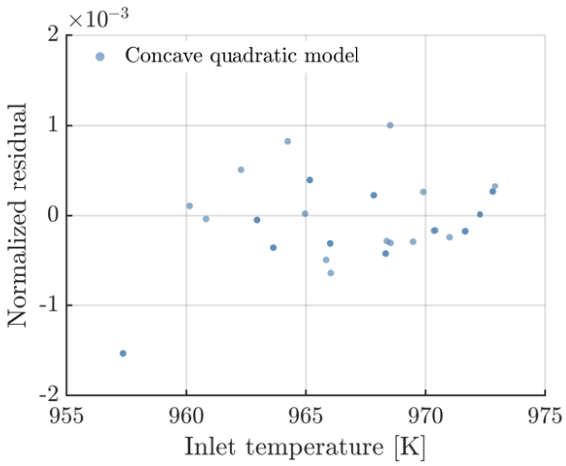


(b) Top of climb

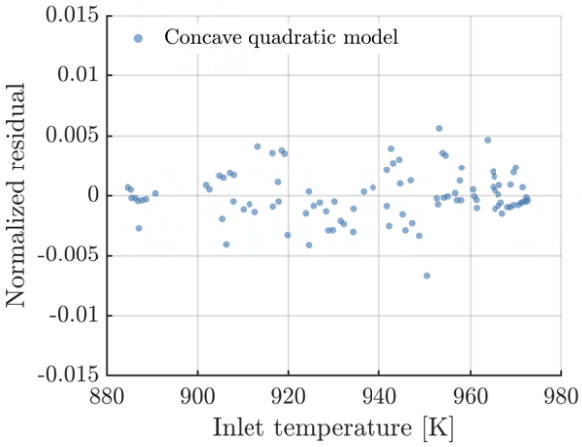


(c) Cruise

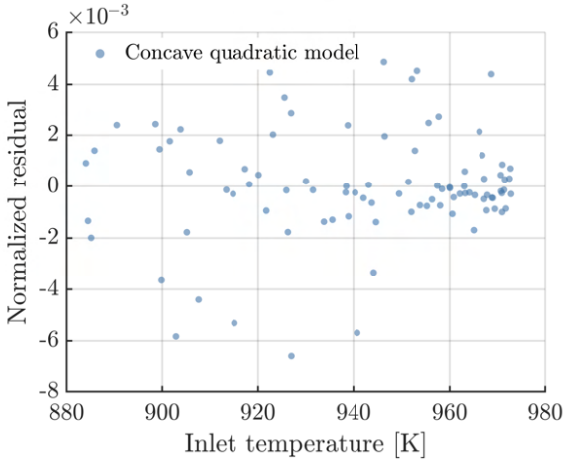
Figure 2 – The SOFC inlet temperature map with respect to power allocation across flight phases.



(a) Take off

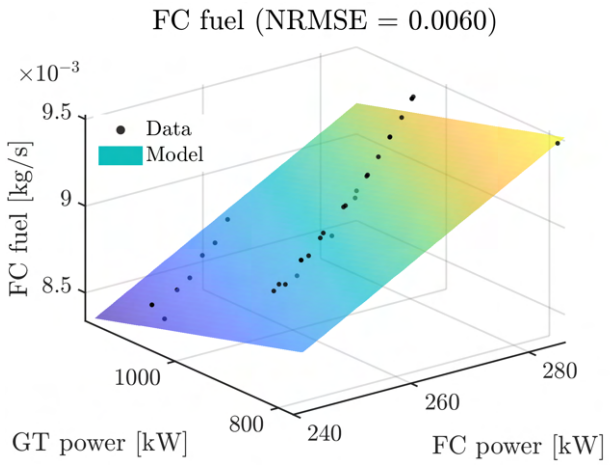


(b) Top of climb

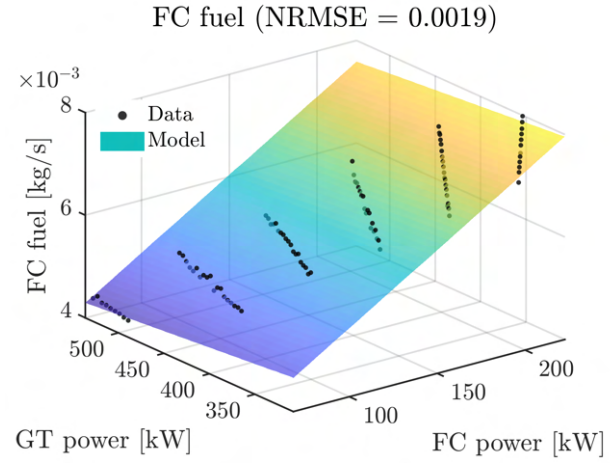


(c) Cruise

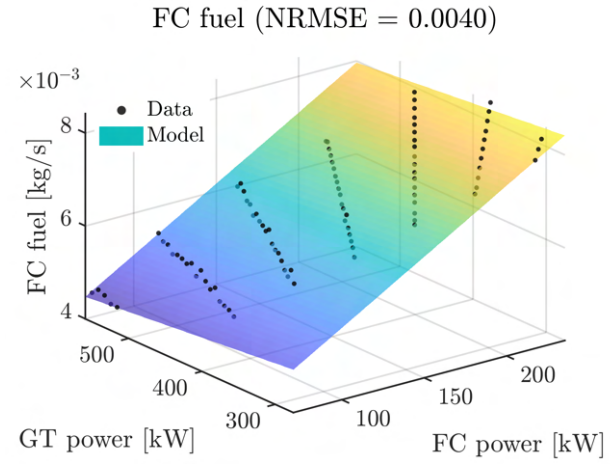
Figure 3 – The SOFC inlet temperature model residual error scatter plots across flight phases.



(a) Take off

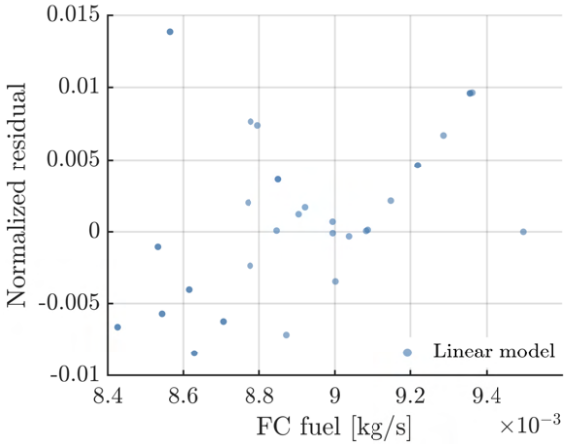


(b) Top of climb

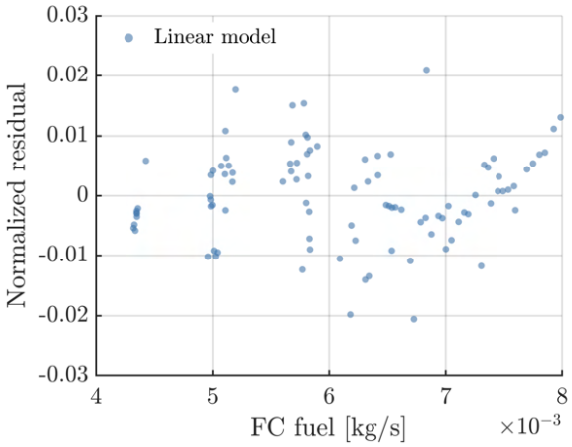


(c) Cruise

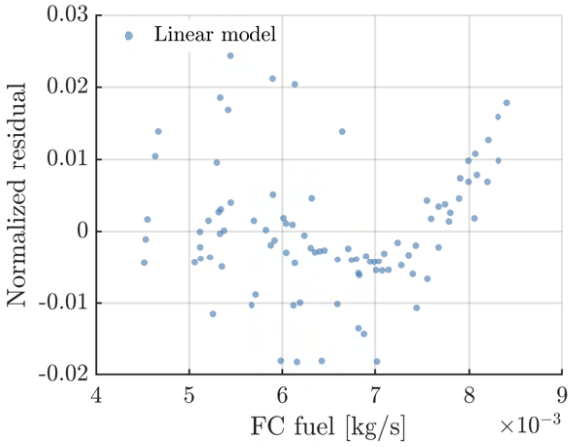
Figure 4 – SOFC fuel flow rate maps as function of GT power and FC power across flight phases.



(a) Take off

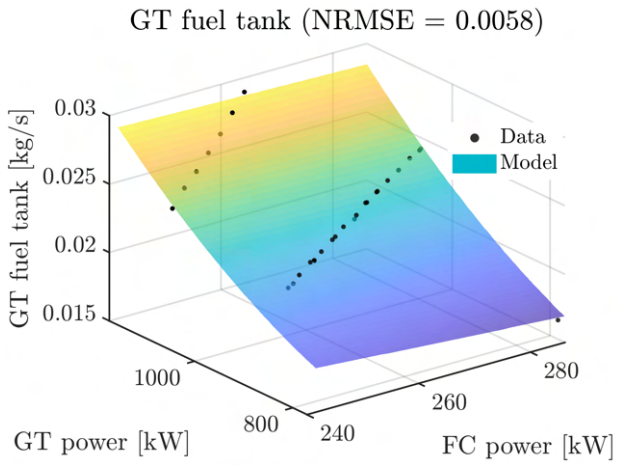


(b) Top of climb

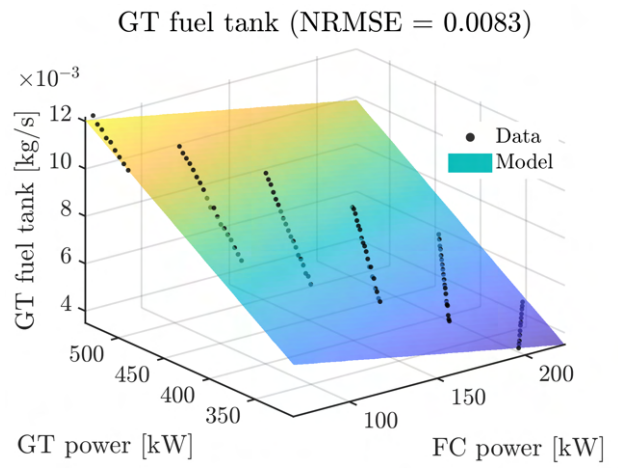


(c) Cruise

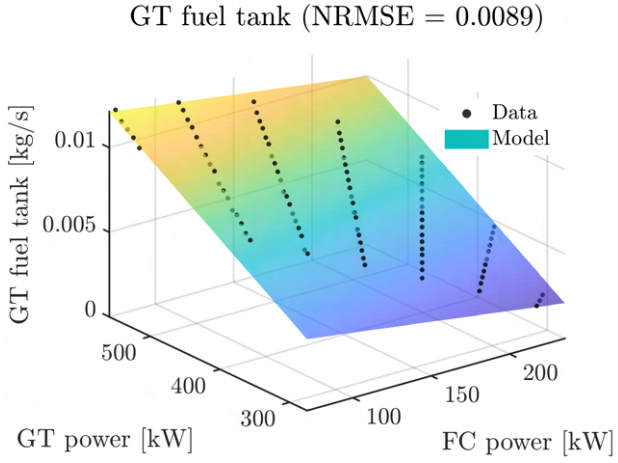
Figure 5 – The SOFC fuel mass flow rate model residual error scatter plots across flight phases.



(a) Take off

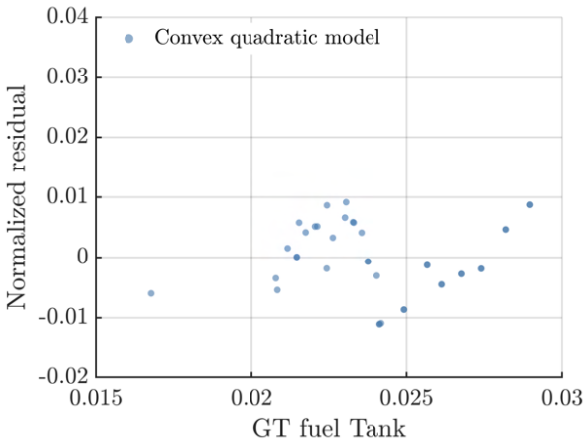


(b) Top of climb

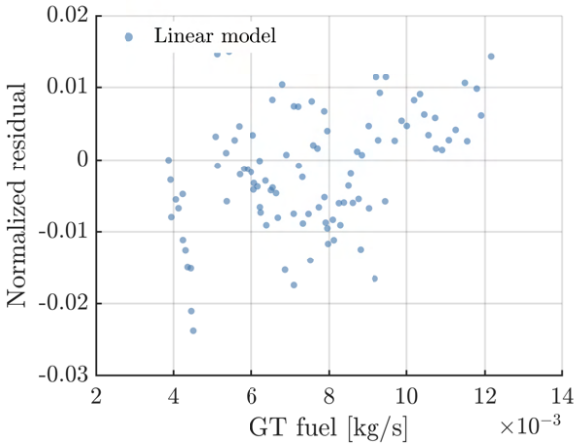


(c) Cruise

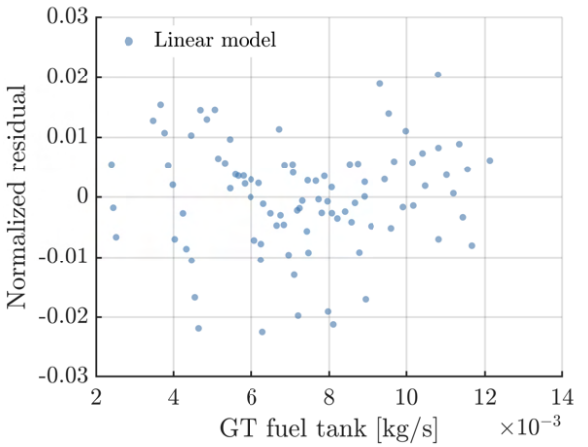
Figure 6 – Gas turbine fuel flow rate maps as function of GT power and FC power across flight phases.



(a) Take-off



(b) Top of climb



(c) Cruise

Figure 7 – The gas turbine fuel mass flow rate model residual error scatter plots across flight phases.

To validate the models, Figs. 3, 5 and 7 present the scatter plots of the normalized residual errors of the surrogate models for key lifting variables across take off, top of climb and cruise conditions as

$$r_{\mathrm{e}} = \frac{(x - \hat{x})}{x_{\max}}, \tag{6}$$

where $\hat{x}$ is the estimated value of the variable from the approximation models and $x_{\max}$ is the maximum value from the dataset for each variables. The residual analysis shows that across all variables and flight phases, the residuals are centered around zero and exhibits no discernible bias, indicating that the surrogate models fo not systematically over or under predict the behavior of the system. Moreover, the absence of visible patterns in Figs. 3, 5 and 7 suggests that the order of the system and nonlinearities are sufficiently captured. These surface maps demonstrate that the surrogate models not only achieve sufficient accuracy but also capture relevant physical trends required for the optimal controller.

2.3 Problem Formulation

The objective is to minimize the fuel consumption over a given time horizon $t \in [0, T]$ during each flight phase,

$$\min \int_0^T \dot{m}_{\mathrm{f}} \, \mathrm{d}t, \tag{7}$$

where $\dot{m}_{\mathrm{f}} = \dot{m}_{\mathrm{f,gt}} + \dot{m}_{\mathrm{f,fc}}$ denotes the combined fuel flow rate to the gas turbine and the fuel cell. The required propulsion power is enforced through the power balance in the integrated propulsion system,

$$P_{\mathrm{req}} = P_{\mathrm{gt}} + \eta \cdot (P_{\mathrm{fc}} - P_{\mathrm{aux}}). \tag{8}$$

Here, the P_{req}, P_{aux} and η are the required power, auxiliary power, and electrical motor efficiency, respectively. These quantities are assumed to be known. Based on the quasi-static models in Eqs. (4) to (8), together with the safety and operational constraints of the propulsion system, the optimal control problem is framed in Problem 1.

Problem 1 (Feedforward optimal control problem)**.** *Given a power request, P_{req}, the optimal power to be provided by GT and SOFC results from the solution of:*

$$\begin{aligned}
&\min_{P_{\mathrm{fc}}} \int_0^T \dot{m}_{\mathrm{f}} \, dt \\
&\text{s.t. Eqs. (4), (5) and (8),} \\
&\quad P_{\mathrm{gt}} \in [P_{\mathrm{gt,min}}, P_{\mathrm{gt,max}}], \\
&\quad P_{\mathrm{fc}} \in [P_{\mathrm{fc,min}}, P_{\mathrm{fc,max}}], \\
&\quad P_{\mathrm{em}} \in [P_{\mathrm{em,min}}, P_{\mathrm{em,max}}], \\
&\quad T_{\mathrm{in}} \in [T_{\mathrm{in,min}}, T_{\mathrm{in,max}}], \\
&\quad T_{\mathrm{hpc}} \in [T_{\mathrm{hpc,min}}, T_{\mathrm{hpc,max}}], \\
&\quad T_{\mathrm{et}} \in [T_{\mathrm{et,min}}, T_{\mathrm{et,max}}], \\
&\quad T_{\mathrm{out}} \in [T_{\mathrm{out,min}}, T_{\mathrm{out,max}}], \\
&\quad \dot{m}_{\mathrm{f,gt}} \in [\dot{m}_{\mathrm{f,gt,min}}, \dot{m}_{\mathrm{f,gt,max}}], \\
&\quad \dot{m}_{\mathrm{f,fc}} \in [\dot{m}_{\mathrm{f,fc,min}}, \dot{m}_{\mathrm{f,fc,max}}], \\
&\quad \dot{m}_{\mathrm{b}} \in [\dot{m}_{\mathrm{b,min}}, \dot{m}_{\mathrm{b,max}}].
\end{aligned} \tag{9}$$

The decision variable in this problem is the fuel cell output power P_{fc}, such that the Problem 1 reduces to a one dimensional optimization problem. Because the system model is purely algebraic and does not include dynamics, the optimization in Problem 1 reduces to a pointwise steady state problem. The resulting control action is therefore computed offline or online as a static optimal control input for each operating point. The Eq. (7) defines the total hydrogen consumption minimized by the optimal

controller, while Eq. (8) enforces the power balance between mechanical and electrical subsystems. The remaining constraints in Eq. (9) represent thermal, mechanical and operational limits. Although the SOFC inlet temperature surrogate is concave, its dependence on the fuel-cell power is monotonic over the admissible operating region. Consequently, the constraint $T_{\text{in}} \leq T_{\text{in,max}}$ is equivalent to an upper bound on P_{fc}. This reformulation preserves convexity of the feasible set and allows the resulting optimization problem to be solved using convex optimization methods and guarantees optimality.

3. Methodology

To derive a closed-form supervisory power management policy, we formulate the Lagrangian of Problem 1 and apply the KKT optimality conditions [18]. For convex optimization problems, these conditions are both necessary and sufficient for optimality and consists of stationarity, primal feasibility, dual feasibility, and complementary slackness. Since no system dynamics are included, the resulting policy does not provide feedback adaptation but represents a computationally efficient feedforward control input evaluated independently at each operating point.

Based on the Problem 1, the system model using Eqs. (4) to (5) are expressed using convex functions together with the constraints on power, temperatures, and mass flow rate variables. Considering the monotonicity of the non convex quadratic constraints, the resulting problems admits a convex feasible set. This structure results in explicit expressions for the optimal fuel cell power at each operating point without iterative numerical solvers. The unconstrained optimum corresponds to the minimum fuel consumption obtained by neglecting system constraints, which equals to

$$P^*_{\text{fc,unc}} = \begin{cases} \frac{2(Q_{\text{f11}}\eta - Q_{\text{f12}})(P_{\text{req}} + \eta P_{\text{aux}}) + (b_1 + q_{\text{f1}})\eta - (q_{\text{f2}} + b_2)}{2(Q_{\text{f11}}\eta^2 - 2Q_{\text{f12}}\eta + Q_{\text{f22}})} & \text{if take off,} \\ +\infty & \text{if top of climb and cruise.} \end{cases} \tag{10}$$

However, feasibility is determined with respect to the operational and thermal constraints. Therefore, if $P^*_{\text{fc,unc}}$ lies beyond the feasible set, KKT conditions guarantee that the optimal solution occurs at an active constraint. The KKT conditions associated with Problem 1 are given as

$$\frac{\partial L}{\partial P_{\text{fc}}} = 0, \tag{11}$$

$$\mu_i \cdot g_i = 0, \tag{12}$$

$$\mu_i \geq 0, \tag{13}$$

$$g_i \leq 0, i = 1, 2, 3, ..., 18, \tag{14}$$

where Eq. (11) denotes the stationary condition, Eq. (12) is the complementary slackness, Eq. (13) is the dual feasibility, and Eq. (14) is the primal feasibility. The constraint vector $\mathbf{g}$ collects the operational boundaries on lifting variables as well as the powers and inputs. We define the corresponding Lagrangian as

$$L = \dot{m}_{\text{f,fc}} + \dot{m}_{\text{f,gt}} + \boldsymbol{\mu}^\top \cdot \mathbf{g} \tag{15}$$

where μ denotes the vector of Lagrange multipliers associated with the inequality constraints. Applying the stationary condition with respect to the decision variable P_{fc} gives

$$\frac{\partial L}{\partial P_{\text{fc}}} = \frac{\partial(\dot{m}_{\text{f,fc}} + \dot{m}_{\text{f,gt}})}{\partial P_{\text{fc}}} + \boldsymbol{\mu}^\top \frac{\partial \mathbf{g}}{\partial P_{\text{fc}}}, \tag{16}$$

which leads to a piecewise analytical expression for the optimal power management policy after implementing Eq. (12)- Eq. (14). As a result, when only affine constraints are active, the optimal value follows the closed form expression of

$$P^*_{\text{fc,lin}} = \frac{x_{j,\max/\min} - \theta_{j,0} - \theta_{j,1}(P_{\text{req}} + \eta P_{\text{aux}})}{-\theta_{j,1}\eta + \theta_{j,2}} \tag{17}$$

and if a quadratic constraint is active then the optimal power for fuel cell is obtained from the scalar quadratic root as

$$P^*_{\text{fc,quad}} = \frac{-b_j \pm \sqrt{b_j^2 - 4a_j c_j}}{2a_j}, \tag{18}$$

with coefficients

$$a_j = Q_{j,22} - 2Q_{j,12}\eta + Q_{j,11}\eta^2, \tag{19}$$
$$b_j = 2(Q_{j,12} - \eta Q_{j,11})(P_{\text{req}} + \eta P_{\text{aux}}) - q_{j,1}\eta + q_{j,2}, \tag{20}$$
$$c_j = Q_{j,11}(P_{\text{req}} + \eta P_{\text{aux}})^2 + q_{j,1}(P_{\text{req}} + \eta P_{\text{aux}}) + q_{j,0} - x_{j,\max/\min}. \tag{21}$$

Therefore, when a linear constraint is active, the optimal fuel cell power reduces to the affine expression in Eq. (17). Similarly, when a quadratic constraint is active, like the inlet temperature limit, the optimal power is obtained by solving a scalar quadratic equation.
Applying the KKT stationary condition shows that the dominant active constraint is the SOFC inlet temperature upper bound in all three phases. Consequently, the corresponding optimal control policy is given by the inequality constraint of the T_{in} upper bound, which leads to

$$P^*_{\text{fc,const}} = \frac{-b + \sqrt{b^2 - 4ac}}{2a}, \tag{22}$$

where

$$a = Q_{22} - 2Q_{12}\eta + Q_{11}\eta^2, \tag{23}$$
$$b = 2(Q_{12} - \eta Q_{11})(P_{\text{req}} + \eta P_{\text{aux}}) - q_1\eta + q_2, \tag{24}$$
$$c = Q_{11}(P_{\text{req}} + \eta P_{\text{aux}})^2 + q_1(P_{\text{req}} + \eta P_{\text{aux}}) + q_0 - T_{\text{in,max}}, \tag{25}$$

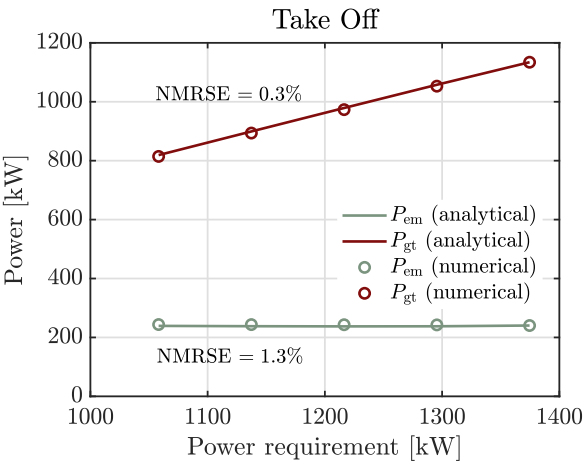
where Q, $\mathbf{q}$ and q_0 are the mapping coefficients of the T_{in} model. Eventually, the optimal policy is

$$P_{\text{fc,opt}} = \min\{P_{\text{fc,const}}, P_{\text{fc,unc}}\}. \tag{26}$$

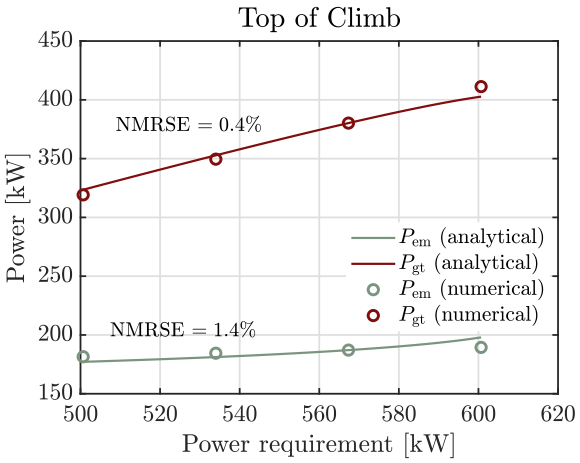
The full calculations and methodology are described in the extended version of the paper [19].

4. Results

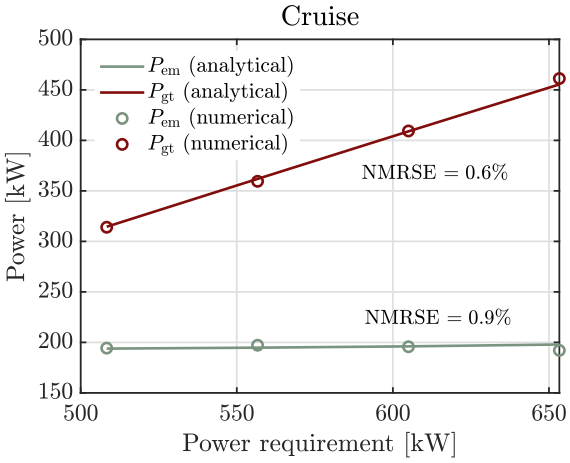
To validate the proposed analytical control policy, we compare the resulting power split with the result from the numerical NLP based power management strategy [20] , for all three phases and over a representative range of power demands. We show the comparison in Fig. 8, which presents the distribution of power between the gas turbine subsystem and the electrical components along a range of total power requirement during different flight phases. As the power requirement increases, the gas turbine power increases approximately linearly, while the electrical motor power remains almost constant in all three phases. Showing that the electrical motor power is primarily constrained by the SOFC inlet temperature rather than being affected by the total power demand. However, take-off requires substantially higher power demand than cruise and top of climb and larger part of the power is provided by the gas turbine rather than the electrical power source. The analytical results closely matches the numerical results, which confirms that the simplified models that have been used for analytical solution are sufficient for the power management problem. Figure 9 shows the corresponding overall fuel consumption of the propulsion system. As the power requirement increases the fuel consumption is also rising linearly in cruise and top of climb phases. The fuel flow rate in take off shows a weakly convex monotonic increase, which was expected from the quadratic fuel flow rate map for GT. As the power requirement is higher in take off than the other phases, the fuel consumption is higher than in cruise and top of climb. Comparing the results from the analytical control policy with the numerical optimal strategy, the NRMSEs are less than 0.7% for fuel consumption and less than 1.5% for power allocation, confirming that the analytical solution provides an accurate approximation over the relevant operating range.



(a) Take off

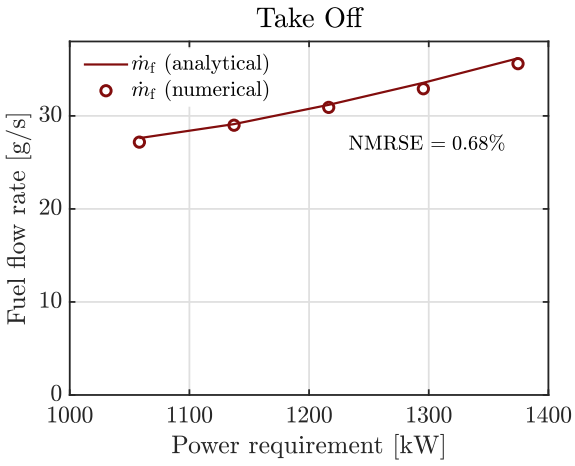


(b) Top of climb

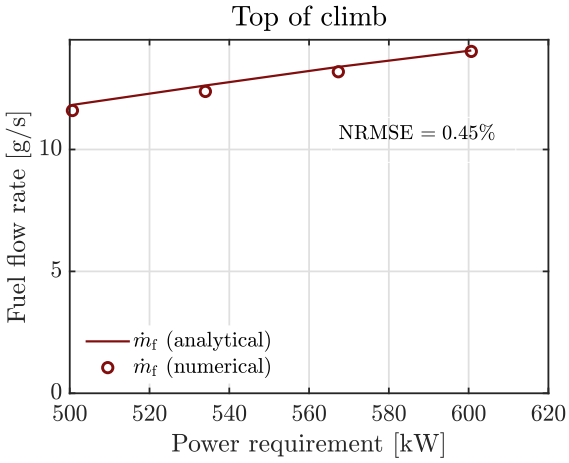


(c) Cruise

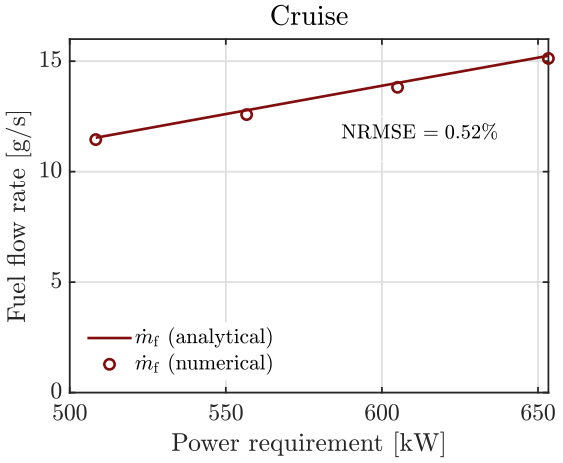
Figure 8 – Power split between subsystems for different power requirements across flight phases.



(a) Take off

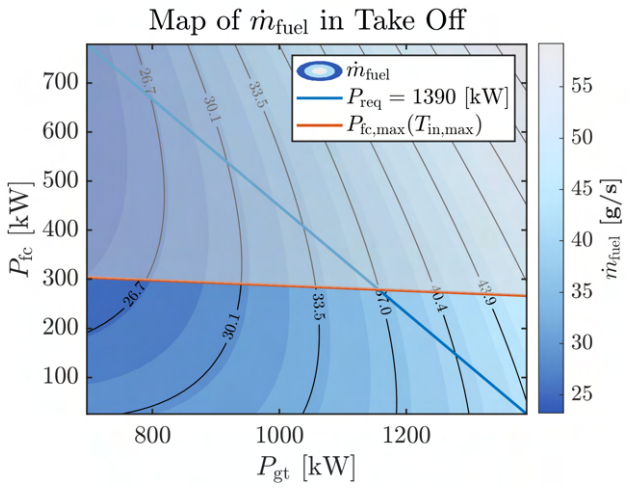


(b) Top of climb

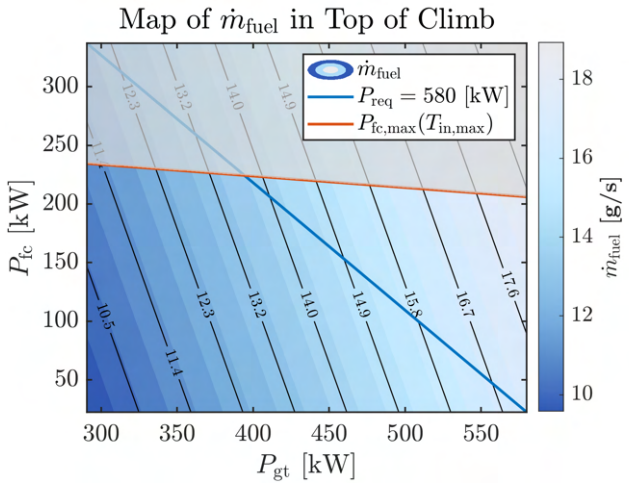


(c) Cruise

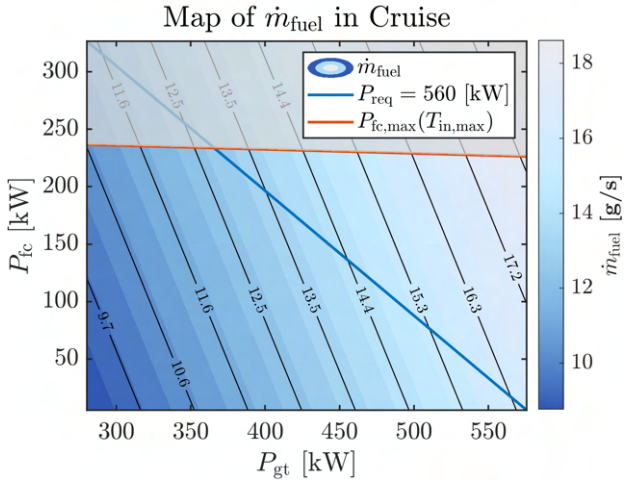
Figure 9 – Fuel flow rate for different power requirements across flight phases.



(a) Take off



(b) Top of climb



(c) Cruise

Figure 10 – Fuel flow rate contour maps for different flight phases. In each phase the constant power requirement is drawn in blue line to show how different power split affects the fuel consumption.

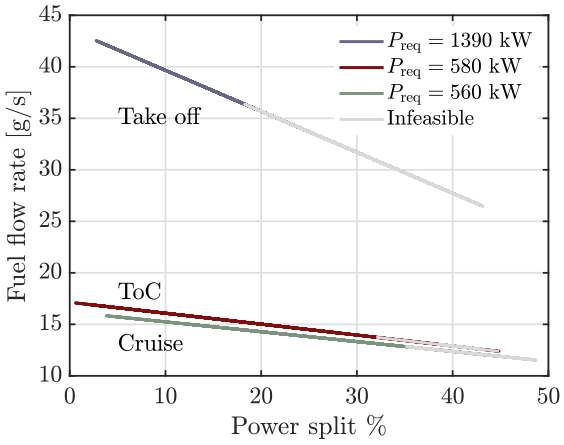
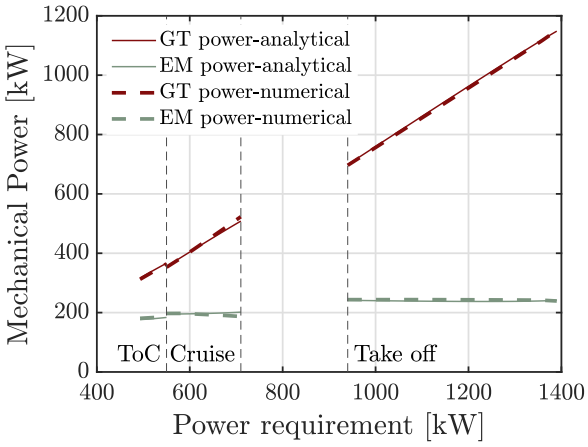
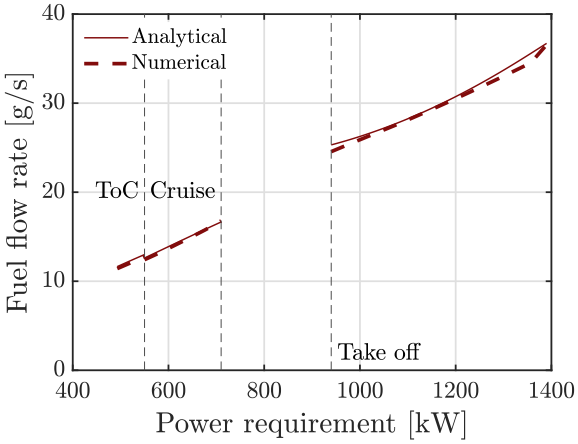


Figure 11 – Fuel flow rate changes with respect to different power split schemes with three fixed power requirements.



(a) Power split for different power requirements



(b) Fuel flow rate for different power requirements

Figure 12 – Comparison of power split and fuel flow rate for different power requirements.

The fuel flow rate maps in Fig. 10 illustrates the fuel consumption as function of gas turbine power and fuel cell power representing linear changes for top of climb and cruise and the quadratic behavior in take off. The maximum admissible fuel cell power is constraint by the fuel cell inlet temperature constraint and it is depicted as $P_{\text{fc,max}}$. The contour plots show the feasible combination of gas turbine and fuel cell power that satisfy a given constant power requirement in each flight phase. The minimum fuel flow rates consistently occur along the upper bound for the fuel cell power resulting from the SOFC inlet temperature upper bound, which is interpreted that the fuel optimal operation is achieved by operating the SOFC at its maximum allowable power and supplying the remaining power demand with the gas turbine. This confirms that the optimal solution shows boundary seeking behavior with respect to the inlet temperature upper bound.
Moreover, Fig. 11 further illustrates the effect of power split on fuel consumption for three fixed total power requirements. The results show that increasing the fuel cell power consistently reduces the overall fuel flow rate, which is caused due to the higher efficiency of the SOFC compared to GT. However, this trend holds up to the maximum admissible fuel cell power, constrained by its inlet temperature. Any additional power demand beyond that is supplied by the GT.
To validate the policy performance during all phases, we show the comparison between the powersplit result by the analytical policy with the numerical result with high fidelity models in Fig. 12. The figure shows an acceptable precision in results for the desired power ranges for all three phases, despite the simple models that were utilized. At each operating point, the proposed static feedforward power management policy yields optimal power setpoints that closely match the numerical steady state optimal solution.
The optimal powersplit in Fig. 12a depicts that the share of the electrical motor power during different flight phases all together. In terms of computational efficiency, solving the optimization problem for 360 different data points, the numerical optimization requires 214.23 s, whereas the analytical method requires 0.81 s. Both computations were performed in MATLAB on a computer equipped with a 12th Gen Intel® Core™ i7-12700H (2.30 GHz) processor and a 16.0 GB of RAM, highlighting the computational advantage of the analytical approach.

5. Discussion and Future Work

While the current work establishes a theoretical foundation for the analytical optimal control policy in the hybrid propulsion system, future research will focus on implementing and validating this policy under steady-state operating conditions. Since the result highlights the critical role of the SOFC thermal constraints, future work will expand the problem formulation to incorporate thermal dynamics, which can introduce nonlinearities and require dynamic optimal control methods, such as using model predictive control (MPC).

6. Conclusion

In this paper we developed an analytical supervisory power management policy for a hydrogen based hybrid aero engine combining a gas turbine and a solid oxide fuel cell. The study focused on three steady-state operating conditions during take off, top of climb and cruise. This framework is an analytical static feedforward optimal control law for the steady state operation. To facilitate the offline calculations of the analytical solution, we used quasi-static approximation to identify the surrogate models of the integrated propulsion system that captures the thermodynamic and power relationships algebraically while preserving convexity and monotonicity characteristics for each operating point.
Based on the resulted models, we formulated an optimal control problem and solved it analytically by utilizing KKT conditions, leading to a closed form power management policy without requiring iterative numerical procedures. The analytical policy was validated against an NLP based approach using high fidelity propulsion model. Across all studied flight phases and considered power ranges, the analytical results closely matched the numerical solutions, with small errors in power split and fuel flow rates. These findings support that the proposed reduced order modeling and the analytical optimal control framework are suitable for the feedforward supervisory power management in hybrid propulsion system while ensuring the optimality according to the feasibility domain set. While the present formulation does not include dynamic feedback, the resulting feedforward power management structure provides a foundation for future extensions toward dynamic optimal control.

Acknowledgment

In this paper, we used Microsoft Copilot as an editor tool.

7. Contact Author Email Address

The corresponding author email address for further contact is f.pak@tue.nl.

8. Copyright Statement

The authors confirm that they, and/or their company or organization, hold copyright on all of the original material included in this paper. The authors also confirm that they have obtained permission, from the copyright holder of any third party material included in this paper, to publish it as part of their paper. The authors confirm that they give permission, or have obtained permission from the copyright holder of this paper, for the publication and distribution of this paper as part of the ICAS proceedings or as individual off-prints from the proceedings.

References

[1] FlyECO. Future enabling technologies for hydrogen-powered electrified aero engine for clean aviation. Available online at `https://flyeco-european-project.eu/`, 2024.

[2] D. San Benito Pastor, E. Pontika, S. de Graaf, D. Ewald, A. Weber, S. Kazula, M. Ferrari, and P. Laskaridis. Hydrogen-powered integrated power and propulsion system (ipps) architecture for sustainable aviation: Leveraging synergies between gas turbine and solid oxide fuel cells. *Towards Sustainable Aviation Summit (TSAS)*, 2025.

[3] O. Cots, J. Gergaud, and D. Goubinat. Direct and indirect methods in optimal control with state constraints and the climbing trajectory of an aircraft. *Optimal Control Applications and Methods*, 2018.

[4] T. Sun, X. M. Sun, and A. Sun. Optimal output tracking of aircraft engine systems: A data-driven adaptive performance seeking control. *IEEE Transactions on Circuits and Systems II: Express Briefs*, 2021.

[5] S. Liu, Y. Shi, T. Sun, P. Li, and X. Zhao. Transient-state adaptive optimal control of aircraft engine systems with input saturation. *IEEE Transactions on Aerospace and Electronic Systems*, 2024.

[6] V. Zaccaria, D. Tucker, and A. Traverso. Transfer function development for sofc/gt hybrid systems control using cold air bypass. *Applied Energy*, 2016.

[7] B. Restrepo, L.E. Banta, and D. Tucker. Simulation of model predictive control for a fuel cell/gas turbine power system based on experimental data and the recursive identification method. In *Proc. ASME Fuel Cell Science, Engineering and Technology Conference*, 2016.

[8] S. Kameswaran, L.T. Biegler, S. T. Junker, and H. Ghezel-Ayagh. Optimal off-line trajectory planning of hybrid fuel cell/gas turbine power plants. *AIChE journal*, 2007.

[9] X. Mi, J. Wen, S. Xiao, X. Sun, X. Jia, Y. Weng, S. Weng, and X. Lv. Quick-safe intelligent control strategy for sofc/gt all-electric ship propulsion system under pulsed load using eo-nn approach. *Energy*, 2025.

[10] Z. Dimitrova and F. Maréchal. Environomic design for electric vehicles with an integrated solid oxide fuel cell (sofc) unit as a range extender. *Renewable energy*, 2017.

[11] S. N. Motapon, L. A. Dessaint, and K. Al Haddad. A comparative study of energy management schemes for a fuel-cell hybrid emergency power system of more-electric aircraft. *IEEE Transactions on Industrial Electronics*, 2013.

[12] J. Chen, M. Liang, H. Zhang, and S. Weng. Study on control strategy for a sofc-gt hybrid system with anode and cathode recirculation loops. *International Journal of Hydrogen Energy*, 2017.

[13] R. Wang and S. M. Lukic. Dynamic programming technique in hybrid electric vehicle optimization. In *2012 IEEE International Electric Vehicle Conference*, 2012.

[14] A. Rezaei, J. B. Burl, and B. Zhou. Estimation of the ecms equivalent factor bounds for hybrid electric vehicles. *IEEE Transactions on Control Systems Technology*, 2017.

[15] K. R. Bouwman, T.H. Pham, S. Wilkins, and T. Hofman. Predictive energy management strategy including traffic flow data for hybrid electric vehicles. *IFAC-PapersOnLine*, 2017.

[16] T. Hofman, M. Steinbuch, R.M. van Druten, , and A.F.A. Serrarens. Rule-based energy management strategies for hybrid vehicle drivetrains: A fundamental approach in reducing computation time. *IFAC Proceedings Volumes*, 2006. 4th IFAC Symposium on Mechatronic Systems.

[17] MOSEK ApS. Mosek optimizer api. Available online at `https://www.mosek.com`, 2025. Version 11.0.14.

[18] S. S. Rao. *Engineering optimization: theory and practice*. John Wiley & Sons, 2019.

[19] F. Pak, U. Perra, F. Willems, T. Hofman, and M. Salazar. An optimal power management policy for hydrogen-based hybrid aero engines. *ArXiv preprint*, 2026.

[20] U. Perra, F. Pak, E. Pontika, S. Bhapkar, D. Ewald, D. Buzzola, T. Hofman, F. Willems, and M. Salazar. Optimization models and steady-state minimum-fuel operating strategies for hydrogen-based hybrid electric aerospace propulsion systems. *Arxiv preprint*, 2026.